Crosstalk and EMI on microwave circuit boards

by

Todd William Rider

B.S., Kansas State University, 2015

A THESIS

submitted in partial fulfillment of the requirements for the degree

MASTER OF SCIENCE

Department of Electrical and Computer Engineering
College of Engineering

KANSAS STATE UNIVERSITY
Manhattan, Kansas

2017

Approved by:

Major Professor
William B. Kuhn

Copyright

Notice: This manuscript has been authored using funds under the Honeywell Federal Manufacturing & Technologies under Contract No. DE-NA-0002839 with the U.S. Department of Energy. The United States Government retains and the publisher, by accepting the article for publication, acknowledges that the United States Government retains a nonexclusive, paid-up, irrevocable, world-wide license to publish or reproduce the published form of this manuscript, or allow others to do so, for United States Government purposes.

Abstract

Crosstalk and electromagnetic interference (EMI) are constant problems in the design of RF circuits. There have been several studies to analyze and improve isolation of transmission lines, but the focus has been mainly on digital circuits or the isolation goals have been on the order of 40-60 dB. When the isolation goals are much more stringent, such as 80-100 dB, much of a designer's time is still spent ensuring that a circuit meets isolation and EMI constraints. This typically involves the use of extensive metal shielding over a circuit board.

This thesis presents results from an isolation and EMI study to provide a simple reference that can be applied to typical substrates, provided proper scaling is used between substrates. The results in this thesis are reported from DC to 30 GHz using a low cost 4-layer FR4 process. The changes in isolation between various transmission lines types are investigated while varying line separation and length. It is shown that isolation between ground-backed coplanar waveguide (GBCPW) and stripline traces can reach 100dB through L-band and 60dB through Ku-band for 1.3in traces separated by 150mils.

Due to the heavy usage of filters in RF design, the isolation between edge-coupled bandpass filters is also studied. It is seen that isolation levels of 100dB through L-band by enclosing the filters within stripline technology is possible, provided that signal launches and layer transitions are carefully designed. Within the passband of the 20 GHz filter tested, the isolation is less but is still significantly improved by use of enclosed stripline. Lastly, a preliminary assessment of EMI is presented which focuses on radiation levels as well as variables that can degrade isolation performance.

The data illustrated in this thesis can provide guidance in the early stages of RF circuit design to determine appropriate structures to meet given design requirements. It also helps to

assess the degree to which additional metal shielding can be avoided in PC board systems that use multi-layer technologies.

Table of Contents

List of Figures

List of Tables

Acknowledgements

I would like to give a special thank you to Dr. Bill Kuhn for allowing me to join this research endeavor and for all of your help throughout. The time and advice you have given me over the course of my undergraduate and graduate careers is invaluable, thank you.

I would also like to thank my committee members, Dr. William Hageman and Dr. Jungkwun Kim, for taking on the responsibility of advisors as well your useful feedback concerning my work. It is very much appreciated, thank you.

Chapter 1 - Background and Introduction

1.1 - Crosstalk and EMI in Modern Electronics

Addressing crosstalk and electromagnetic interference (EMI) has been a challenge in electronics for decades. From amplifiers to mixers, keeping circuits isolated is key to improving the performance of RF systems. Crosstalk is the coupling of a signal from one part of a circuit to another part of a circuit through electric and/or magnetic fields. EMI is the radiation of RF signals from the circuit into the environment. Through reciprocity, the amount of radiation from a circuit also indicates how susceptible the circuit is from outside interference, so crosstalk and EMI can be related.

The standard technique for mitigating crosstalk and EMI is to use metal shielding with chambers made for each RF circuit on a board. Examples of commercial shielding can be seen in Figure 1.1. While this technique works, the metal housings introduce additional cost, increase product size, and potentially add significant weight to products.

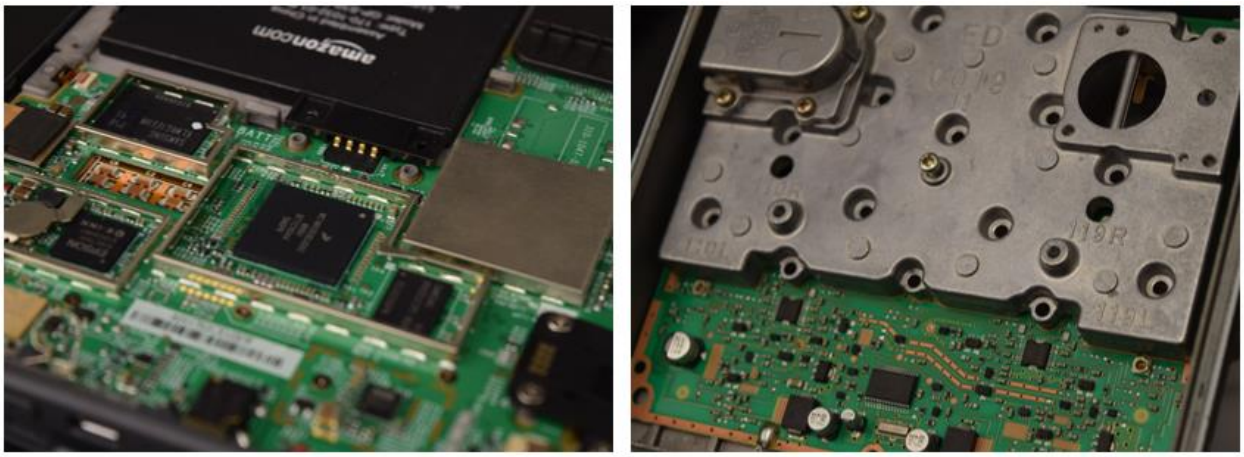

Figure 1.1 Commercial Shielding of Electronics.

With the proliferation of multilayer PCB technologies and accurate characterization of circuit board materials, the use of such shielding can potentially be reduced or eliminated. This

requires careful design and the use of more elaborate structures than the classic PC board trace above an internal ground plane. In the RF field, this is essentially a microstrip transmission line. By applying more carefully considered interconnects such as ground-backed coplanar waveguide (GBCPW) or stripline, a designer should be able to improve crosstalk and EMI through the shielding that results. While the proper design of such structures can be costly in terms of employee time when working at microwave frequencies, once the structures are well understood the time spent on their design will decrease, and the use of additional metal shielding could be greatly reduced.

While the use of structures such as stripline or GBCPW provides increased isolation, there is still no easy way to know without prior experience if a given structure will provide enough isolation for a given application without time-consuming simulation and experimental verification. To this end analytical, simulation, and experimental results will be discussed in this thesis to provide a better understanding of achievable crosstalk values without added shielding. The focus will be on how crosstalk varies based on layout variables such as transmission line type, line separation, and line length. Since the use of metal shielding also aims to reduce EMI, the radiation of RF structures will be investigated as well. The main goal of this research is to provide an increased understanding of isolation in RF systems as well as provide isolation trends that can be used to shorten the design cycle of RF circuit boards.

1.2 - Prior Work

There have been extensive analyses done on transmission lines including the study of crosstalk and EMI, particularly in the digital signal domain. In the digital world, the far-end crosstalk (FEXT) of two transmission lines has been the primary focus as it is typically the most

detrimental to circuit operation [1, 2, 3]. Though it's typically less of a concern in such circuits, the near-end crosstalk (NEXT) has also been the topic of several studies [4, 5]. Most of the research articles found employ similar strategies of analyzing crosstalk, such as calculating the even and odd mode capacitances which are used to determine coupling between two lines. Though these papers are useful, there can be constraints on the usable range of the equations used in determining the line characteristics, such as those found in [6, 7]. These constraints seem to be the result of digital line analysis where transmission lines are typically in close proximity due to PC board layout constraints, and isolation goals are not very stringent due to the nature of digital signals. In analog RF circuits, where transmission lines are separated by greater distances, and the crosstalk goals can be much more difficult to achieve, the analyses commonly used provide a level of error due to these constraints and can't be solely relied upon for the design transmission lines.

While some work has been done on RF transmission line isolation, the results usually pertain to simple structures such as directional couplers [8, 9] or differential transmission lines [10], which typically involve closely spaced lines. Studies have also been done on the effects of using via fences between two microstrip lines [11]. This research does not look at the isolation corresponding to large line separation typically found on RF circuit boards and also fails to build trends that can be easily applied to current and future designs.

1.3 - Thesis Organization

This thesis is broken into four chapters. The first chapter provides a brief introduction to RF circuit board isolation, current practices, and prior work that has been done towards crosstalk understanding. The second chapter presents an analysis of coupled microstrip transmission lines. Electromagnetic simulations of coupled transmission lines and coupled filters are also presented.

The third chapter presents an in-depth look at crosstalk on RF circuit boards carried out in this research, particularly focusing on high-frequency crosstalk vs. layout variables such as transmission line spacing, type, and length. The fourth chapter discusses preliminary results from a study on RF radiation from circuit boards and the possibility of radiation reduction without the use of added shielding. Chapter 5 concludes the thesis by providing a brief review and summary of important results as well as suggestions for areas where future work could be conducted. Finally, the appendix provides information on S-Parameters.

Chapter 2 - Analysis and Simulations of Crosstalk

2.1 - Circuit Board Stack-Up

A standard 4 layer stack-up using FR4 was selected for use in this isolation study. This decision was made for several reasons, such as manufacturing cost and time, with the primary factor being that 4 layer FR4 is a standard in the electronics industry. Since the basic physics is not heavily dependent on the material type, the results can be easily extrapolated to new designs and to lower loss substrates such as those made by Rogers Corp, or to low temperature co-fired ceramic (LTCC).

Figure 2.1 shows a standard 4 layer stack-up produced by several circuit board manufacturers. While the specific dimensions and tolerances vary among manufacturers, the general stack-up is the same. In our studies H_1 and H_2 are 8.5mils and 40mils, respectively. The grey via shown in Figure 2.1 is representative of a standard via that traverses all layers of the board. The use of blind or buried vias was avoided in this work due to significant increases in cost.

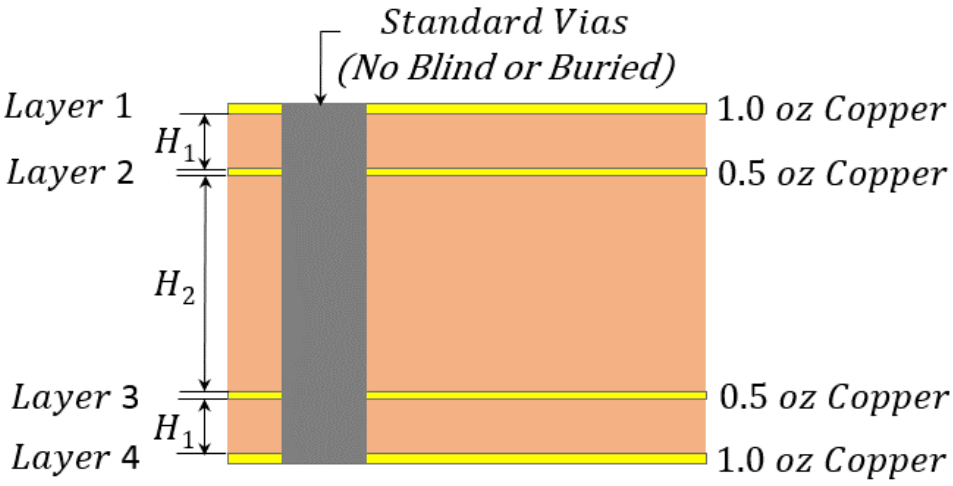

Figure 2.1 Standard 4 Layer Stack-Up.

2.2 - PC Board Transmission Lines Tested

Three types of transmission line were used in these studies. These were microstrip, ground backed coplanar waveguide (GBCPW), and stripline. Figure 2.2 shows the dimensional views of each transmission line structure. In Figure 2.2.c, the red illustrates a signal transition via that connects layer 1 to layer 3. Since blind vias were not used, a 10 mil via stub exists between layers 3 and 4. To maximize isolation, the stripline included sidewalls to enclose it fully within a rectangular chamber. The grey vias in Figure 2.2.c create the walls of the stripline chamber, which is outlined by a dotted line. This type of stripline is sometimes referred to in the literature as enclosed stripline or rectax (rectangular coax) [12].

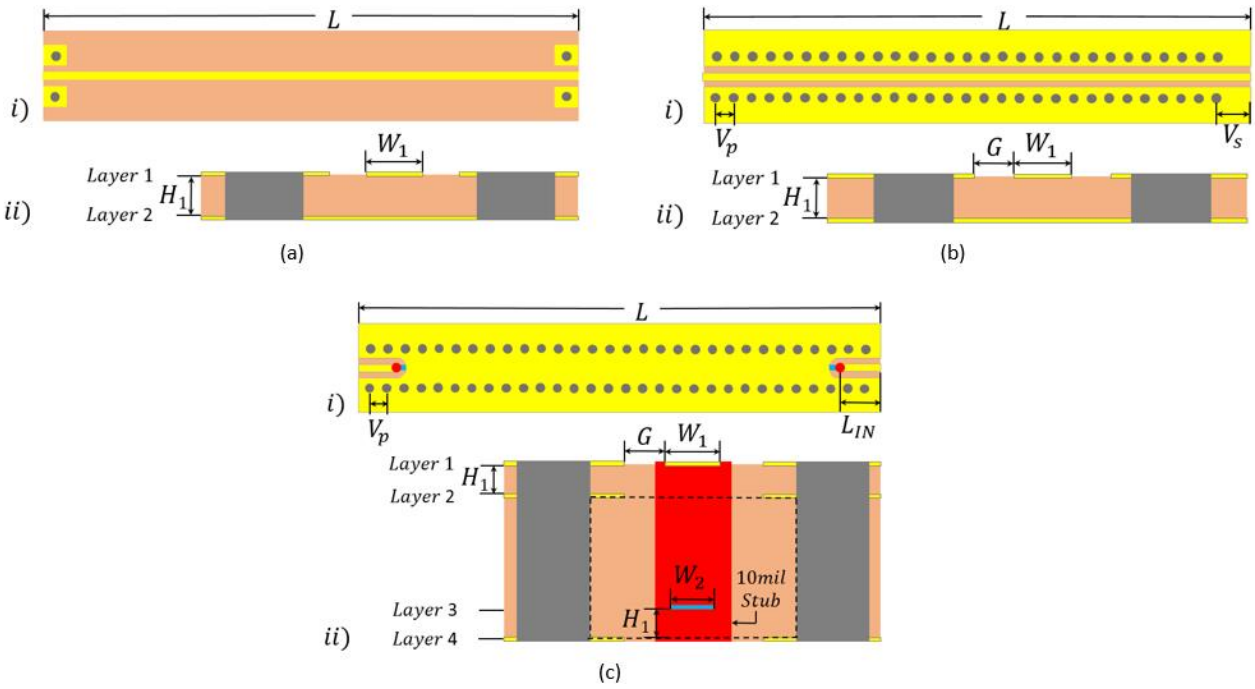

Figure 2.2 Transmission Line Dimensional Views.

a) Microstrip Transmission Line. b) GBCPW transmission line. c) Stripline Transmission line.

i) Top View. *ii*) Cross Section.

Lastly, Table 2.1 provides a summary of the physical dimensions for the various transmission lines used in this study. The dimensions given are used throughout this thesis unless specifically stated otherwise.

Table 2.1 Summary of Transmission Line Dimensions (mils)

	L	**H_1**	**H_2**	**W_1**	**W_2**	**G**	**V_S**	**V_P**	**L_{IN}**
Microstrip	1300	8.5	-	16	-	-	-	-	-
GBCPW	1300	8.5	-	14	-	8	20	20	-
Stripline	1300	8.5	40	14	13	8	10	10	80

2.3 - The Transmission Line Crosstalk Model

Two transmission lines running in parallel to each other will exhibit a mutual capacitance and mutual inductance which allow coupling to occur. For this analysis, the lumped element LC model for a transmission line used in [13] is employed. A simplified five segment example of the model can be seen in Figure 2.3. In this figure, the C values represent the capacitance between each line segment and ground, Cm values represent the mutual capacitance between the two lines, L values represent the self-inductance of each line, Lm values represent the mutual inductance between the lines, V_{xn} values represent the phasor node voltages of each line segment, and Z_o represents a termination equal to the characteristic impedance of the lines.

To calculate the amount of voltage that couples from line A to line B, the superposition property is used. This allows the capacitive coupling, inductive coupling, and resistive losses to be determined independently from one another. A simple lumped element approach is used to solve for the coupling between two microstrip lines. It is important to note, for this approach to be accurate each line segment must represent a length much shorter than the wavelength of the highest frequency of interest. It has been determined that the highest frequency of interest for this study is

30 GHz. The wavelength of a 30 GHz signal in FR4 is approximately 5mm. For this analysis, each line segment will represent 1µm, which is sufficiently small.

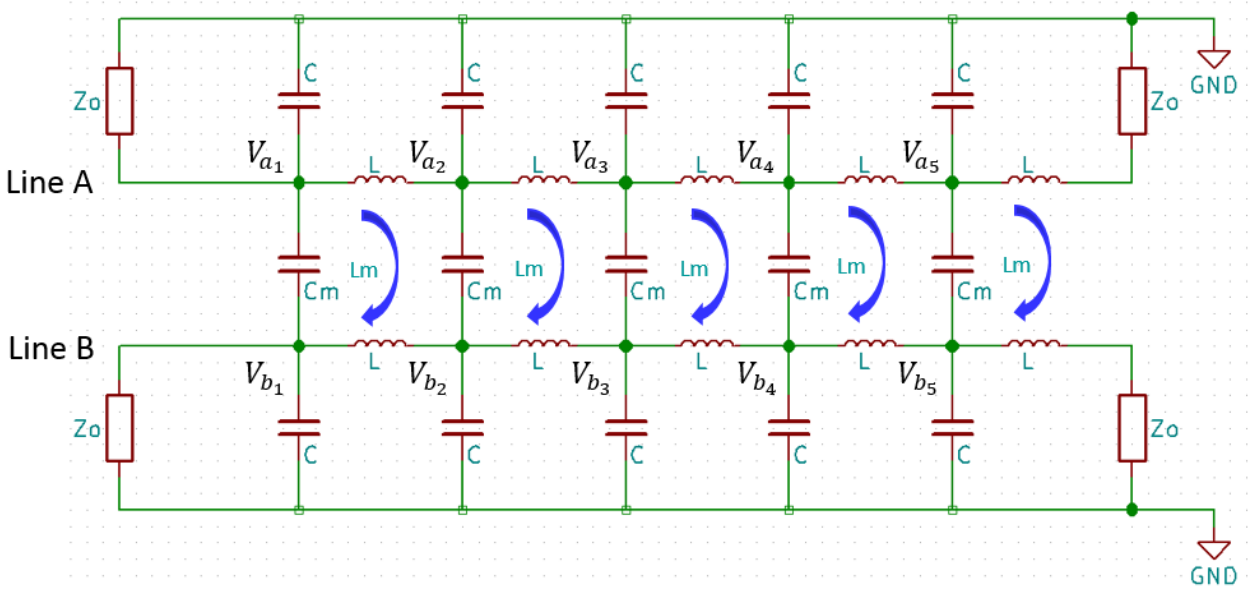

Figure 2.3 Lumped Element Model for Coupled Transmission Lines.

2.3.1 - Capacitively Induced Crosstalk

To assess the capacitive coupling, a voltage divider is used on the equivalent model of an arbitrary segment of the line, shown in Figure 2.4. The relationship between the line voltages is given by (2.1) and (2.2). Assuming that $X_{Cm} >> Z_o$, (2.3) gives a simpler close-approximation of the voltage seen at the adjacent node of line B due to capacitive coupling.

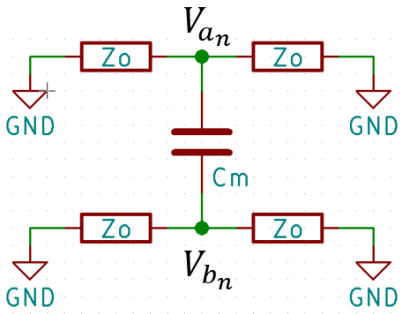

Figure 2.4 Lumped Element Model of Capacitive Coupling.

$$V_{a_n} = V_A e^{j\omega t} \tag{2.1}$$

$$V_{b_n} = V_{a_n}\left(\frac{\left(\frac{Z_O}{2}\right)}{\left(\frac{Z_O}{2}\right)-j\left(\frac{1}{\omega C_m}\right)}\right) = V_{a_n}\left(\left(\frac{\left(\frac{Z_O}{2}\right)^2}{\left(\frac{Z_O}{2}\right)^2+\left(\frac{1}{\omega C_m}\right)^2}\right)+j\left(\frac{\left(\frac{Z_O}{2}\right)\left(\frac{1}{\omega C_m}\right)}{\left(\frac{Z_O}{2}\right)^2+\left(\frac{1}{\omega C_m}\right)^2}\right)\right) \tag{2.2}$$

$$V_{b_n} \approx V_A e^{j\omega t}\left(\frac{Z_O \omega C_m}{2}\right) * j \tag{2.3}$$

To determine the total voltage induced in line B, all additional line segments must also be considered. As a signal travels from $V_{a_1} \rightarrow V_{a_2} \rightarrow V_{b_2}$ and from $V_{a_1} \rightarrow V_{b_1} \rightarrow V_{b_2}$ (see Figure 2.3) an equal phase shift occurs. This means that the coupled signal propagating down line B will add constructively as it approaches the far end. (2.4) gives the total RMS voltage, V_{B_C}, seen at the far end of line B due to capacitive coupling.

$$\left|V_{B_C}\right| \approx \frac{V_A}{\sqrt{2}}\left(\frac{Z_O \omega C_m}{2}\right) * N \tag{2.4}$$

Where N is the total number of line segments.

2.3.2 - Inductively Induced Crosstalk

To determine the inductive coupling, the equivalent model shown in Figure 2.5 is used. In this model, a signal on line A moves from $V_{a_n} \rightarrow V_{a_{n+1}}$ creating a time-varying current, i_{a_n}. Through mutual inductance a current, i_{b_n}, is induced on line B. Using the relationship between voltage and current for an inductor, the voltage $V_{b_{n+1}}$ can be solved in terms of the known voltage on line A. The voltages seen at the nodes of line A are defined in (2.5). The current on line A is then found using (2.6). Then, using (2.6), the voltage across the inductor on line B is found using (2.7).

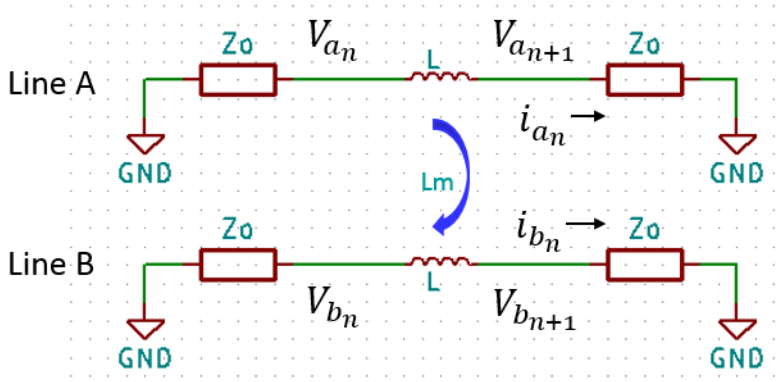

Figure 2.5 Lumped Element Model of Inductive Coupling.

$$V_{a_n} = V_A e^{j\omega t} \quad ; \quad V_{a_{n+1}} = V_A e^{j\omega t+\theta} \tag{2.5}$$

$$V_{a_n} - V_{a_{n+1}} = V_A\left(e^{j\omega t} - e^{j(\omega t+\theta)}\right) = j\omega L i_{a_n} \quad \rightarrow \quad i_{a_n} = -j\frac{V_A}{X_L}\left(e^{j\omega t} - e^{j(\omega t+\theta)}\right) \tag{2.6}$$

$$V_{b_n} - V_{b_{n+1}} = j\omega L_m i_{a_n} = V_A\frac{L_m}{L}\left(e^{j\omega t} - e^{j(\omega t+\theta)}\right) \tag{2.7}$$

The measured signal on line B is the real part of (2.7), which is given in (2.8). Since each line segment represents $1\mu m$, the phase shift, θ, induced by one segment is close to zero. This allows for the close approximations made in (2.9), giving a simple expression for the induced voltage on line B for a single segment.

$$\Re\left(V_{b_n} - V_{b_{n+1}}\right) = V_A\frac{L_m}{L}[\cos(\omega t) - \cos(\omega t + \theta)] \tag{2.8}$$

$$V_A\frac{L_m}{L}[\cos(\omega t) - \cos(\omega t + \theta)] = V_A\frac{L_m}{L}[\cos(\omega t)(1 - \cos(\theta)) - \sin(\omega t)\sin(\theta)] \tag{2.9}$$

$$\approx -V_A\frac{L_m}{L}\sin(\omega t)\,\theta$$

Where $\theta \approx 0$.

Since the induced voltage on a single segment of line B is across $2Z_o$, the current, i_{b_n}, is found using (2.10). The voltage across Z_o is then given by (2.11). As the signal propagates down line A the voltages induced on line B will remain in phase and add linearly, thus yielding (2.12) for the total RMS voltage at the far end of line B due to inductive coupling. Since each segment represents 1μm, the phase shift from V_{b_n} to $V_{b_{n+1}}$ can be found with (2.13).

$$i_{b_n} = \frac{V_{b_n} - V_{b_{n+1}}}{2Z_o} \tag{2.10}$$

$$i_{b_n} Z_o = \frac{V_{b_n} - V_{b_{n+1}}}{2} = -\frac{V_A}{2}\left(\frac{L_m}{L}\right)\sin(\omega t)\,\theta \tag{2.11}$$

$$\left|V_{B_L}\right| \approx \frac{V_A}{2\sqrt{2}}\frac{L_m}{L}\theta * N \tag{2.12}$$

$$\theta = \omega\Delta t \;\; ; \;\; \Delta t = \frac{1}{v_p} l \tag{2.13}$$

Where l is the length of one line segment.

2.3.3 - Resistive Losses of the Transmission Lines

To account for power loss in the traces, the model in Figure 2.6 is used. R_S represents the series resistance of each segment of length l in Figure 2.3. The series resistance varies with frequency due to the skin effect. From [14], the skin depth of a conductor is given by (2.14) and the resistance of each segment is given by (2.15). Since a voltage division occurs across each segment, the total attenuation down one line would be the drop across one segment to the power of N, the number of segments. Because this division occurs down each transmission line, attenuation at the far end of line B is the drop across one node to the power of 2N. The attenuation seen at the far end of line B is given by (2.16). Finally, the total RMS voltage at the far end of line B is given by (2.17).

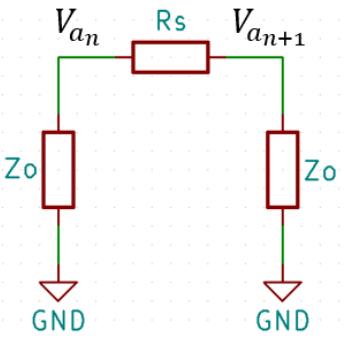

Figure 2.6 Lumped Element Model of Resistive Losses.

$$\delta = \sqrt{\frac{2}{\omega \mu_r \mu_0 \sigma}} \tag{2.14}$$

Where σ is the conductivity, μ_r is the relative permeability, and μ_0 is the permeability of free space.

$$R = \frac{1}{\sigma \delta}\left(\frac{l}{2(W+T)}\right) \tag{2.15}$$

Where l is the segment length, W is the line width, and T is the line thickness.

$$Att = \left(\frac{Z_o}{Z_o + R}\right)^{2N} \tag{2.16}$$

$$\left|V_{B_{tot}}\right| = \left|V_{B_C} + V_{B_L}\right| * Att = \frac{V_A N}{2\sqrt{2}}\left|\omega C_m Z_o - \frac{L_m}{L}\omega \Delta t\right|\left(\frac{Z_o}{Z_o + R}\right)^{2N} \tag{2.17}$$

2.3.4 - Calculated Coupling Values

The final step in this analysis is to calculate the line parameters C, L, C_m, and L_m. To calculate the line parameters, the work of [15] is used along with the eighth chapter of [16]. While calculating the parameters is beyond the scope of this thesis, the equations involved can be found

in [15]. Using (2.17), the expected coupling between two microstrip lines with dimensions from Table 2.1 is shown in Figure 2.7.

In Figure 2.7.a, the coupling decreases by roughly 10-12 dB per doubling of separation. For the 20-40 mil case, the coupling does not follow this trend. When energy moves from line A to line B, the energy on line A is reduced by the same amount. The effect of this is not noticeable until the power on line B becomes comparable to that of line A. Eventually, with appropriate length and separation, all of the energy from A will couple onto line B. This is why the plot appears compressed as the amount of coupling approaches 0dB.

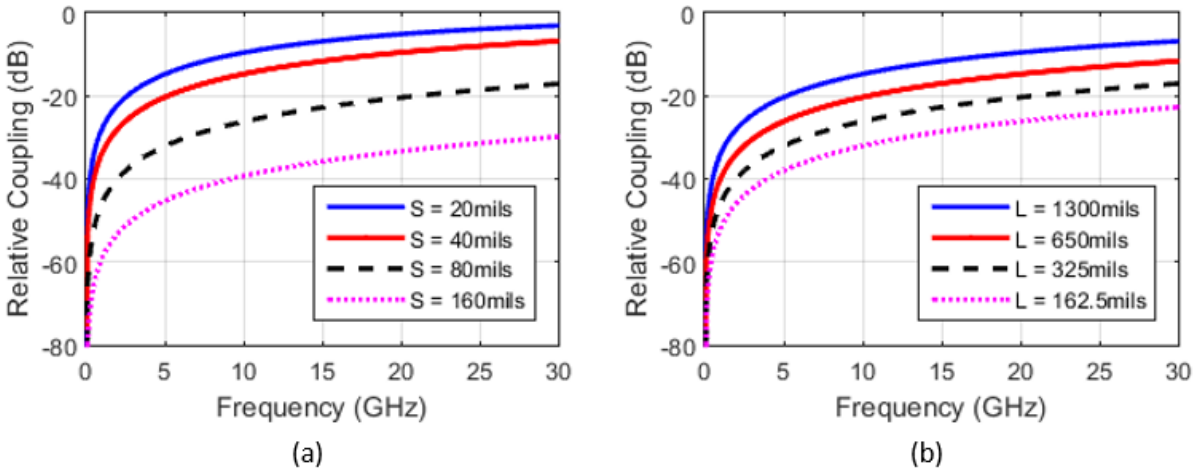

Figure 2.7 Calculated Microstrip Crosstalk.
a) Coupling vs. Spacing (L = 1300mils). b) Coupling vs. Length (S = 40mils).

In Figure 2.7.b, the coupling increases by roughly 5-6 dB per doubling of line length. When varying line length, the per-unit-length line parameters remain the same. Because of this, it is easy to argue that the coupling from line to line varies linearly with line length. When the line length doubles, the power on line B increases by 6dB. This expected behavior is seen in Figure 2.7.b. For very long lines this trend cannot continue. For long lines, the energy on line A will decrease as it couples to line B and the coupling will approach 0dB.

To assess the accuracy of this analysis, these results are compared against the Advanced Design Systems (ADS) schematic simulator. The schematic simulator of ADS is based on equations similar to those derived in this section. Figure 2.8 provides a summary of the ADS results for the same variables used in Figure 2.7. For the case of S = 160 mils, a slight discrepancy between the two figures can be seen. This occurs because a spacing of 160 mils is outside of the suggested range for the equations provided in the appendix. Otherwise, the coupling derived in this section aligns well with the ADS results. This provides support that this analysis, as well as the assumptions made within, are accurate.

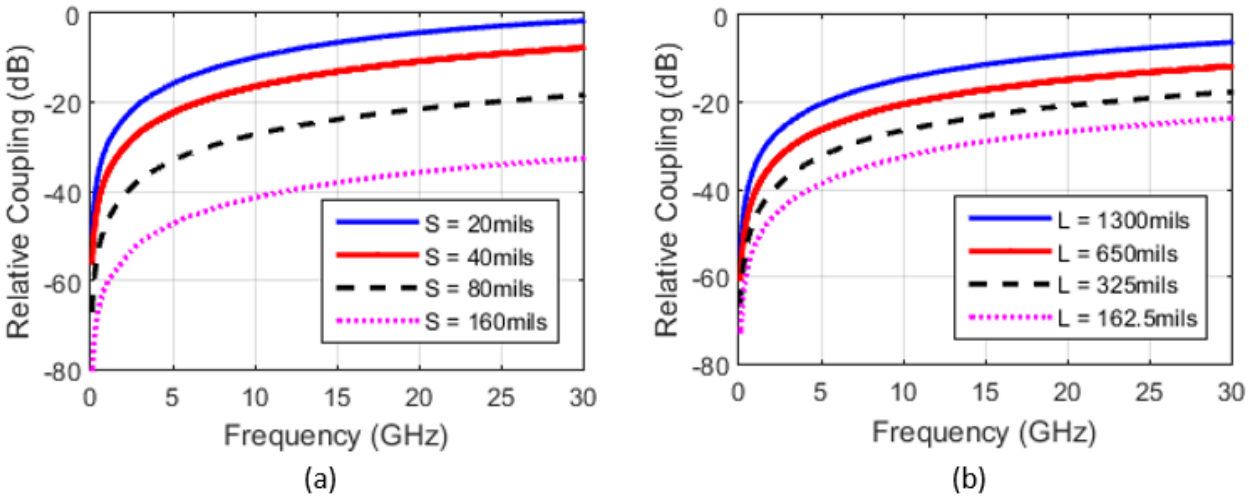

Figure 2.8 Simulated Crosstalk Using ADS Schematic Simulator.
a) Coupling vs. Separation (L = 1300mils). b) Coupling vs. Length (S = 40mils).

2.4 - Simulation of Coupling Levels

Advanced Design Systems was also used to conduct 3-D simulations of coupling levels.

2.4.1 - Coupled Transmission Lines

Because the expected trends for varying separation and length were determined during the analysis, only a single separation and length is considered for each coupling structure. The

transmission line coupling length was L=1300 mils. The separation for both transmission line coupling and filter coupling was S=150 mils. Figure 2.9 provides a summary of the simulated coupling between various transmission lines.

Though the simulated microstrip-microstrip coupling appears to align well with what would be expected based on calculations, there are some discrepancies. This is likely caused by factors such as dielectric loss, surface roughness, and current crowding, which are accounted for in the 3D simulator but not in the calculations. Also, due to the complexity of analyzing C_m and L_m for GBCPW and stripline, the simulator was relied upon for predictions of coupling with these line types. From Figure 2.9.a, by exchanging one or both microstrip lines with GBCPW, the isolation improves by approximately 5dB and 10dB, respectively. In Figure 2.9.b, one GBCPW line was replaced with stripline further improving isolation. These simulations provide support that GBCPW or stripline can significantly improve isolation without added shielding.

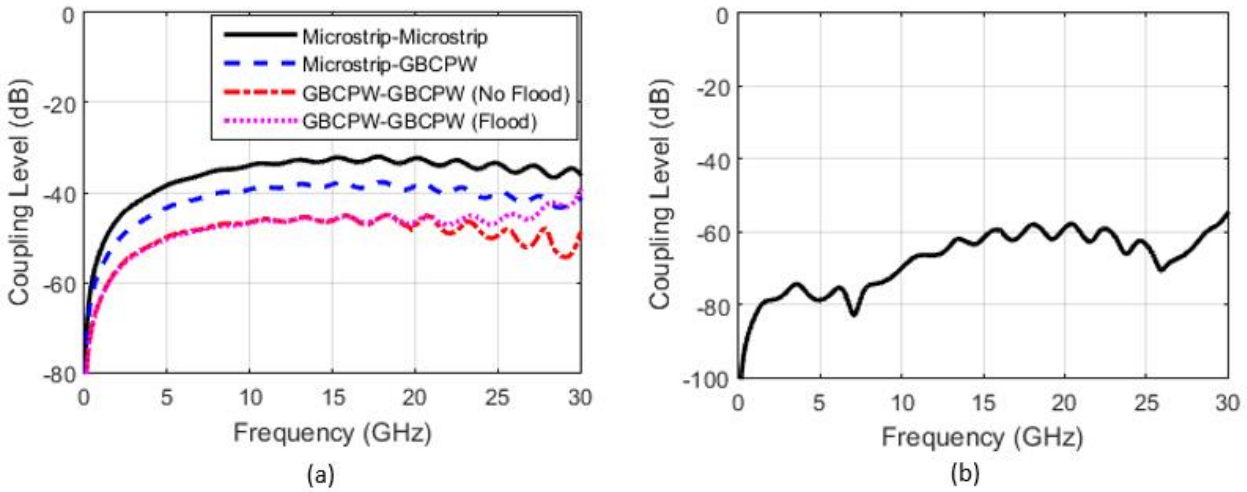

Figure 2.9 Simulated Transmission Line Crosstalk.
a) Microstrip and GBCPW Isolation. b) GBCPW – Stripline Isolation.

Also in Figure 2.9.a, two simulations of GBCPW-GBCPW coupling were conducted. One simulation employed a flooded ground plane on layer 1 between the two lines. The second

simulation did not include a flooded ground plane. This was done because it has become common practice in PC board layout to add a ground flood around circuits to improve performance. This simulation provides support against arbitrarily adding a ground flood as isolation is not improved and even shows degradation at higher frequencies.

2.4.2 - Coupled Filters

Microwave systems often employ bandpass filters as well as transmission lines. Such structures include resonant structures which can increase signal transference and thereby degrade isolation. Hence, filters are also investigated through simulation here and through an experiment in the following chapter. Figure 2.10 shows the layout and simulation of two edge-coupled microstrip filters. The dashed blue line in Figure 2.10.b shows the frequency response of the filters while the solid black line shows the coupling between them. Intuitively, more coupling occurs in the passband of the filter since the edge-coupled structures are resonating at those frequencies. Outside of the passband, only the short microstrip lead-in contributes to the coupling, which is significantly lower.

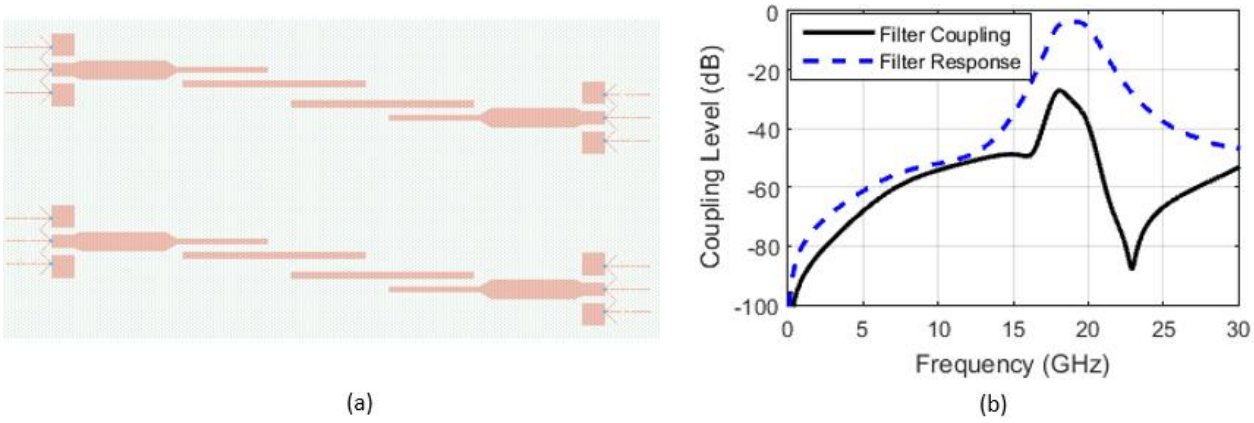

Figure 2.10 Simulated Microstrip Edge-Coupled Filter Crosstalk.
a) Top View of Coupled Filters. b) Filter Crosstalk.

An accurate simulation of two edge-coupled stripline filters was unsuccessful due to limited computing power. Because of this, and other inaccuracies involved with simulations, physical experiments were required to achieve accurate results.

Chapter 3 - Experimental Verification

3.1 - Experimental Setup

Three test boards were used to obtain all of the coupling results presented. Figure 3.1 shows the three test boards that were designed and manufactured for these experiments. The test boards contain transmission line to transmission line coupling test structures with varying distance between the lines as well as varying line length. There are also test structures that allow us to study filter to transmission line coupling and filter to filter coupling. The transmission line structures used are microstrip, GBCPW, and stripline. The filters used are classic edge-coupled microstrip filters and versions of these built with enclosed stripline technology.

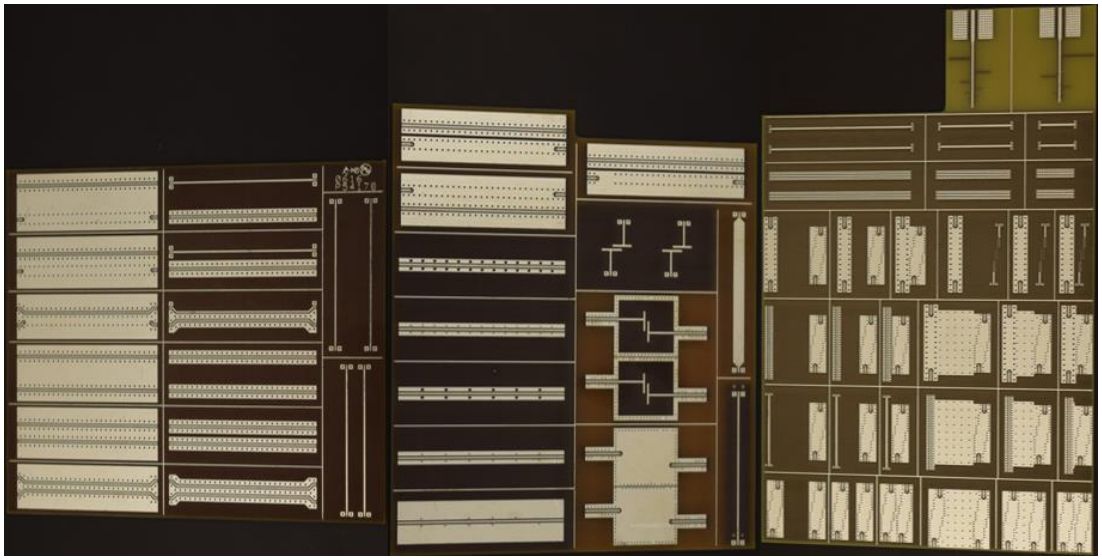

Figure 3.1 Test Boards Used for Coupling Verification.

The measurements were made using a Keysight N5245A network analyzer that works from 10MHz to 50 GHz. The probing was done using GGB Industries Model 40A 500 micron GSG probes that work from DC to 40 GHz. A 2-port calibration was done using a GGB Industries calibration substrate. Figure 3.2 shows the test setup used for the experiments.

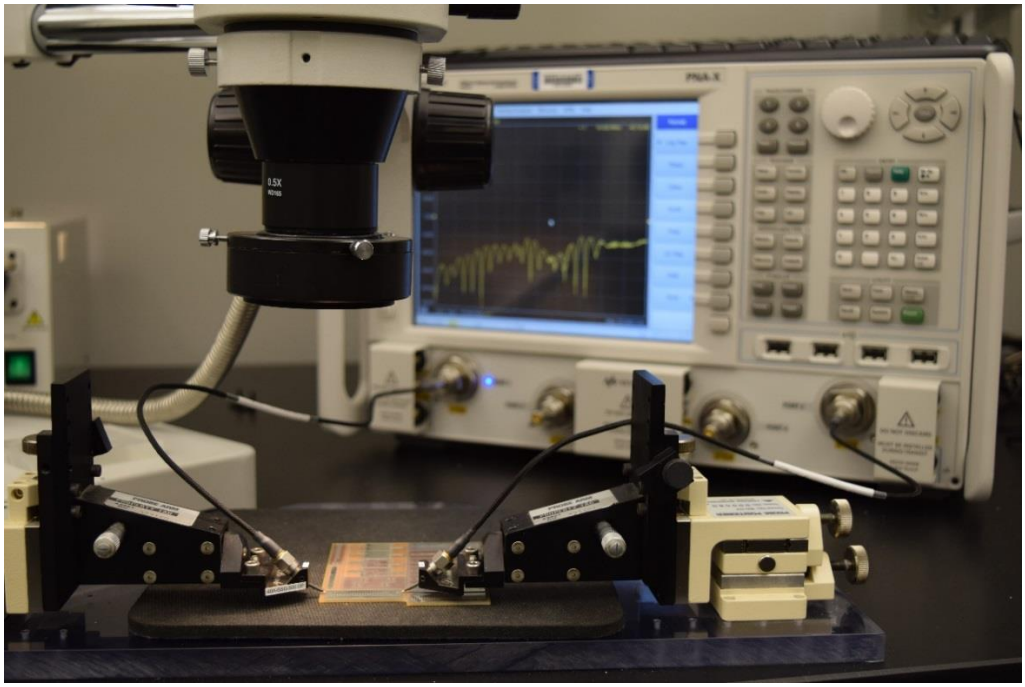

Figure 3.2 Microwave Coupling Test Setup.

3.2 - Measurement of Coupling Levels

The measurement results discussed in this section are split into four subsections. The first subsection looks at the basic response of each microwave structure used in the coupling experiments, to assess line insertion loss and filter response shape. The second subsection presents the transmission line to transmission line coupling results. The third subsection looks at filter to transmission line coupling. Lastly, subsection four considers filter to filter coupling.

3.2.1 - Microwave Structure Frequency Responses

Figure 3.3 shows the frequency response of each transmission line structure. The microstrip and GBCPW responses look nearly identical while the stripline response shows nearly 2dB more loss at 30 GHz. The extra attenuation is caused by decreased line width and increased dielectric loss due to the fact that stripline is fully enclosed by FR4. There is also a small amount of ripple

in the frequency responses, most notably in the stripline response. This ripple is caused by signal reflections on the transmission line. Reflections occur when the characteristic impedance of the transmission line deviates from the ideal 50 ohms, which is likely caused by the signal transition via. For each of the lines, the return loss was verified to be better than 10dB at all frequencies.

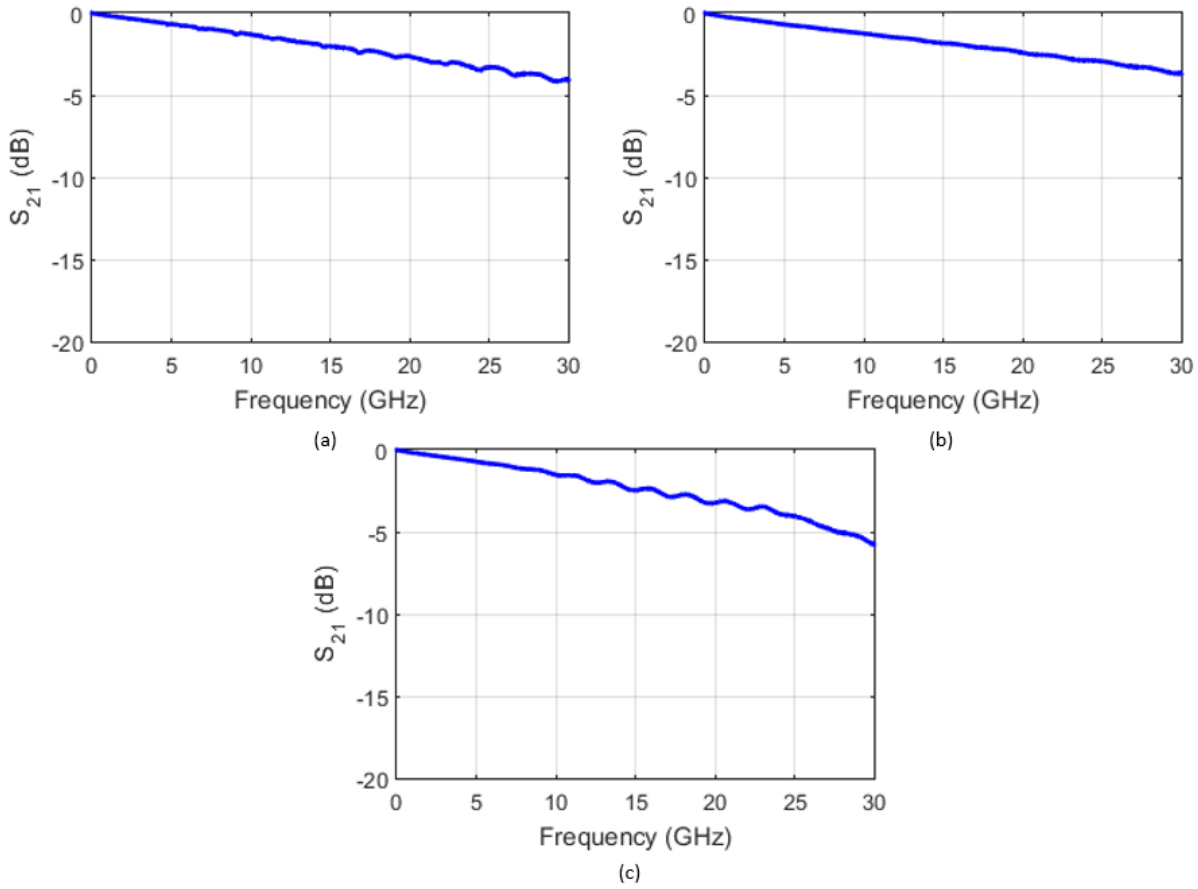

Figure 3.3 Transmission Line Frequency Responses.
a) Microstrip Response. b) GBCPW Response. c) Stripline Response.

Figure 3.4 shows the frequency responses of the two filters used in the coupling experiments, one for filters implemented in microstrip and the other for stripline realizations. The passband of both filters is centered at approximately 21 GHz with a bandwidth of roughly 2 GHz.

Though the passband of the stripline filter is slightly narrower than the microstrip filter, the center frequencies are well aligned. The passband insertion loss of each filter is roughly 5dB.

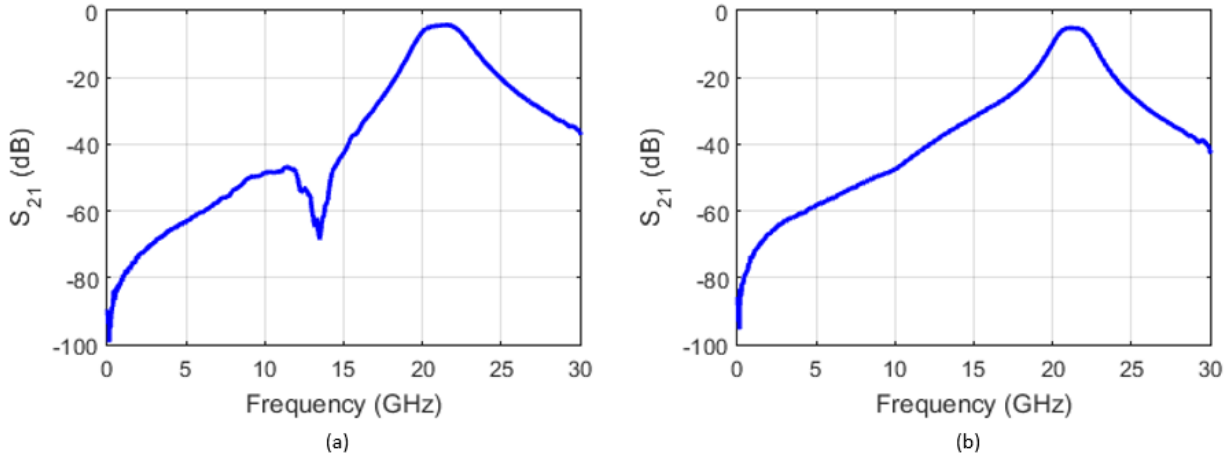

Figure 3.4 Filter Frequency Responses.
a) Microstrip Filter. b) Stripline Filter.

3.2.2 - Transmission Line to Transmission Line Crosstalk

To assess the coupling between lines, adjacent structures were connected between ports 1 and 2 of the network analyzer using the configuration shown in Figure 3.5. Pairs of 0201 sized 100Ω resistors were connected in parallel to make each of the 50Ω terminations shown. The lines were separated by a distance S. For the GBCPW line-pair illustrated, the dotted line represents a ground flood between the structures on the top metal layer. Two sets of coupled GBCPW transmission lines, with and without this ground flood, were included on the test boards. This allows assessment of the effects of ground flooding between structures, a common practice in the RF circuit industry.

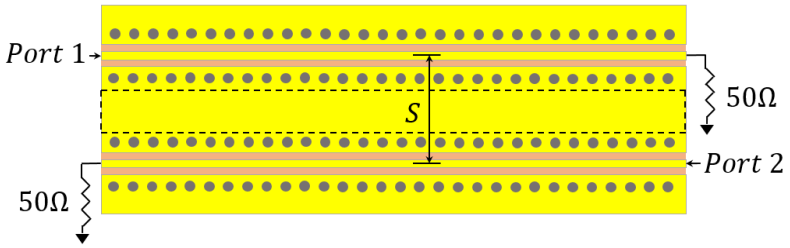

Figure 3.5 Coupling Structure Port Configuration.

The first variable studied was the separation distance, S. Figure 3.6 shows a summary of the far end crosstalk/coupling (FEXT) versus S for various types of coupled lines. The ripples seen for 300 mil spacing are due to signal reflections on the line connected to port 1. The reflections are caused by variations in the characteristic impedance due to manufacturing tolerances. The effect of these reflections becomes more noticeable as the isolation increases.

There are a couple of trends that can be identified from Figure 3.6. First, when using at least one GBCPW transmission line, the isolation shows roughly a 10dB improvement over using two microstrip transmission lines. The second trend, for every doubling of S the isolation shows an improvement of roughly 10dB, which agrees well with the Chapter 2 crosstalk model analysis and simulations.

Figure 3.6.b and Figure 3.6.d show nearly the same isolation levels illustrating that an extra ground flood between GBCPW traces has a minimal impact on the signal isolation. In GBCPW, most of the electric field energy couples from the signal trace to the adjacent ground and then through the vias to the ground below. If proper via stitching is not employed signal degradation can occur, as will be seen in Chapter 4. These results also agree with simulations and provide support against the need to arbitrarily add a ground flood between circuits on a board.

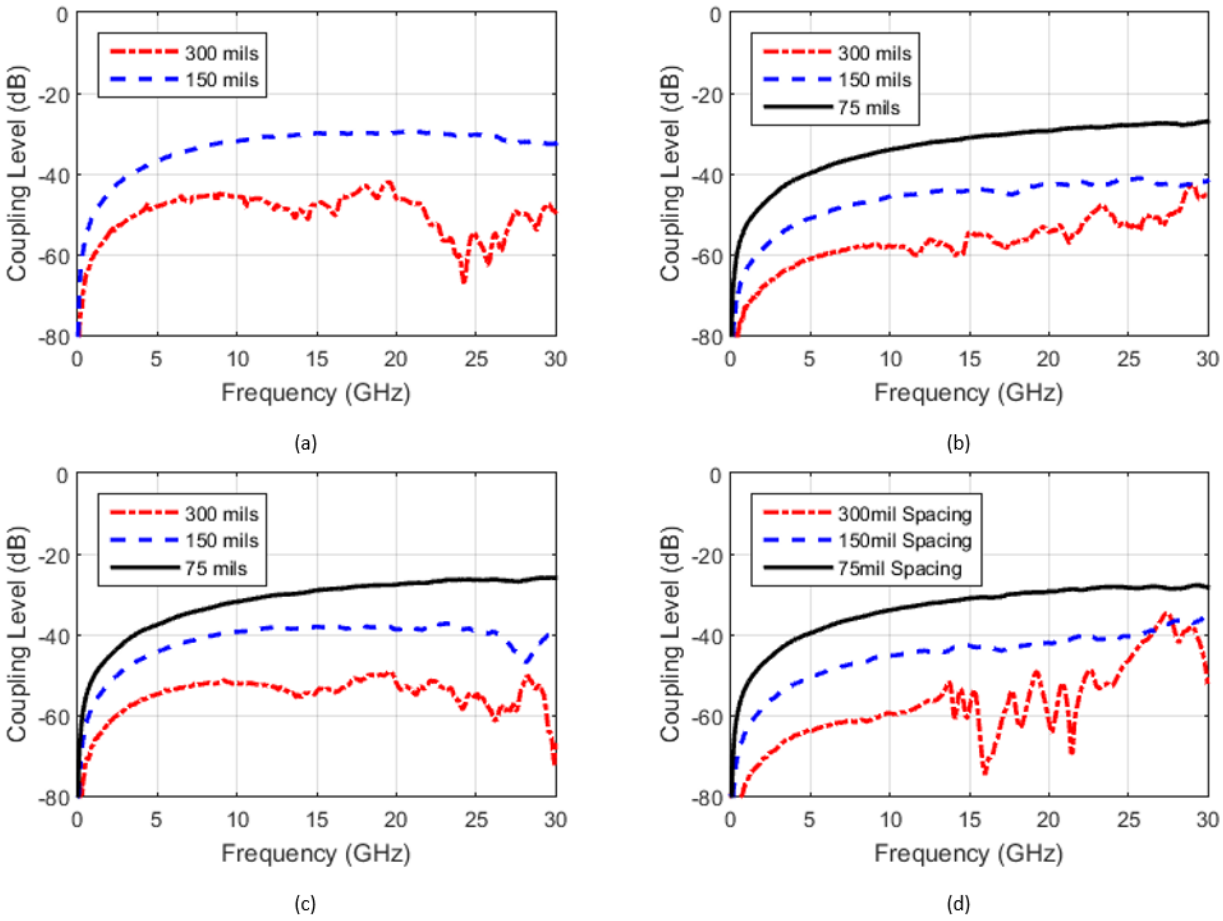

Figure 3.6 Measured Transmission Line Crosstalk vs. Spacing.
a) Microstrip – Microstrip. b) GBCPW – GBCPW w/ GND Flood Between.
c) Microstrip – GBCPW. d) GBCPW – GBCPW w/o GND Flood Between.

Figure 3.7 shows the isolation between stripline and GBCPW with 150 mil spacing between the lines. At lower frequencies, the use of at least one stripline trace improves the isolation by as much as 20dB over GBCPW and 35dB over microstrip alone. At higher frequencies, such as 15 GHz, the isolation improvement is around 20dB relative to GBCPW and 30dB relative to microstrip only implementations. The reduction in isolation at the higher frequencies is believed to be caused by the GBCPW lead-in to the stripline being the main coupling mechanism. Signal reflections caused by the signal transition via may also add to the coupling at higher frequencies.

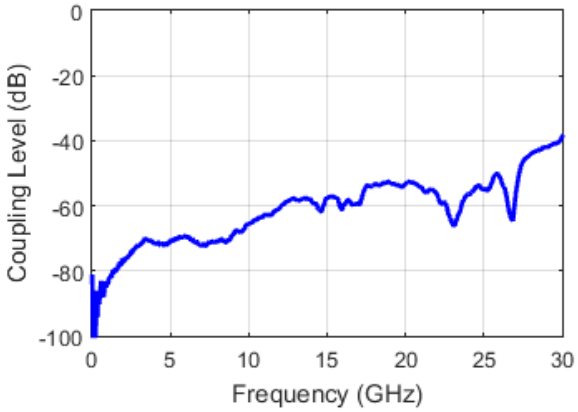

Figure 3.7 Measured Stripline-GBCPW Isolation at 150 mil Spacing.

The second coupling variable studied was the transmission line length, L. Figure 3.8 shows a summary of the FEXT versus L for microstrip and GBCPW coupled lines. For each plot, the separation distance is 150 mils. From Figure 3.8, a trend can be seen that for each doubling of line length the isolation is degraded by about 6dB, which concurs with the results of the lumped model analysis.

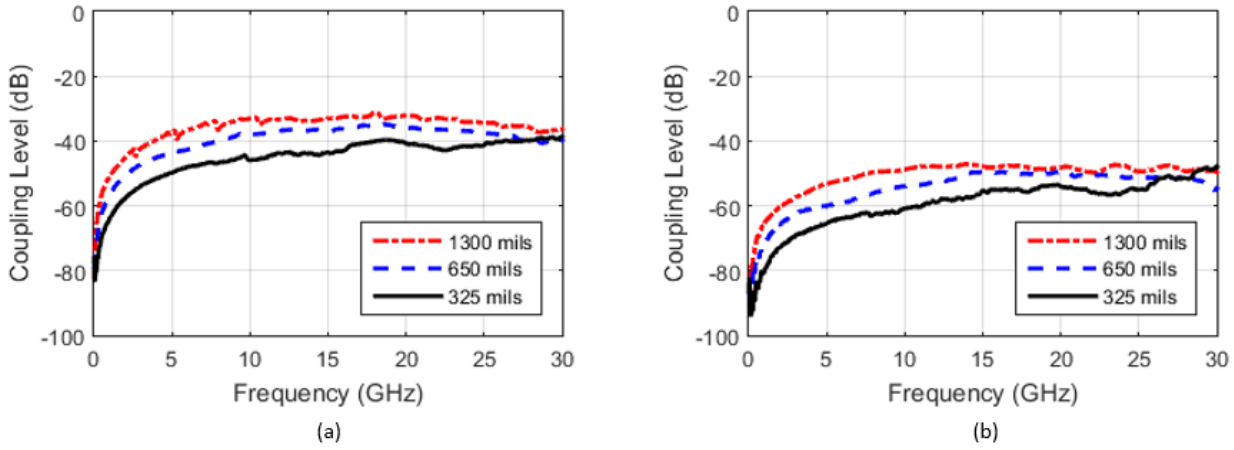

Figure 3.8 Measured Transmission Line Crosstalk vs. Length.
a) Microstrip – Microstrip Isolation. b) GBCPW – GBCPW Isolation.

3.2.3 - Filter to Transmission Line Crosstalk

Figure 3.9 shows microstrip filter to transmission line coupling plots for each of the different transmission lines. The transmission lines and the filters are 650 mils and 600 mils in length, respectively. In Figure 3.9, the same trend for varying distance holds true from the line to line coupling; the isolation improves by roughly 10-12 dB for each doubling of S. Inside the passband of the filter the coupling is increased by roughly 10dB from what you would expect for two coupled transmission lines. While outside of the passband, the coupling behaves roughly the same as two coupled transmission lines.

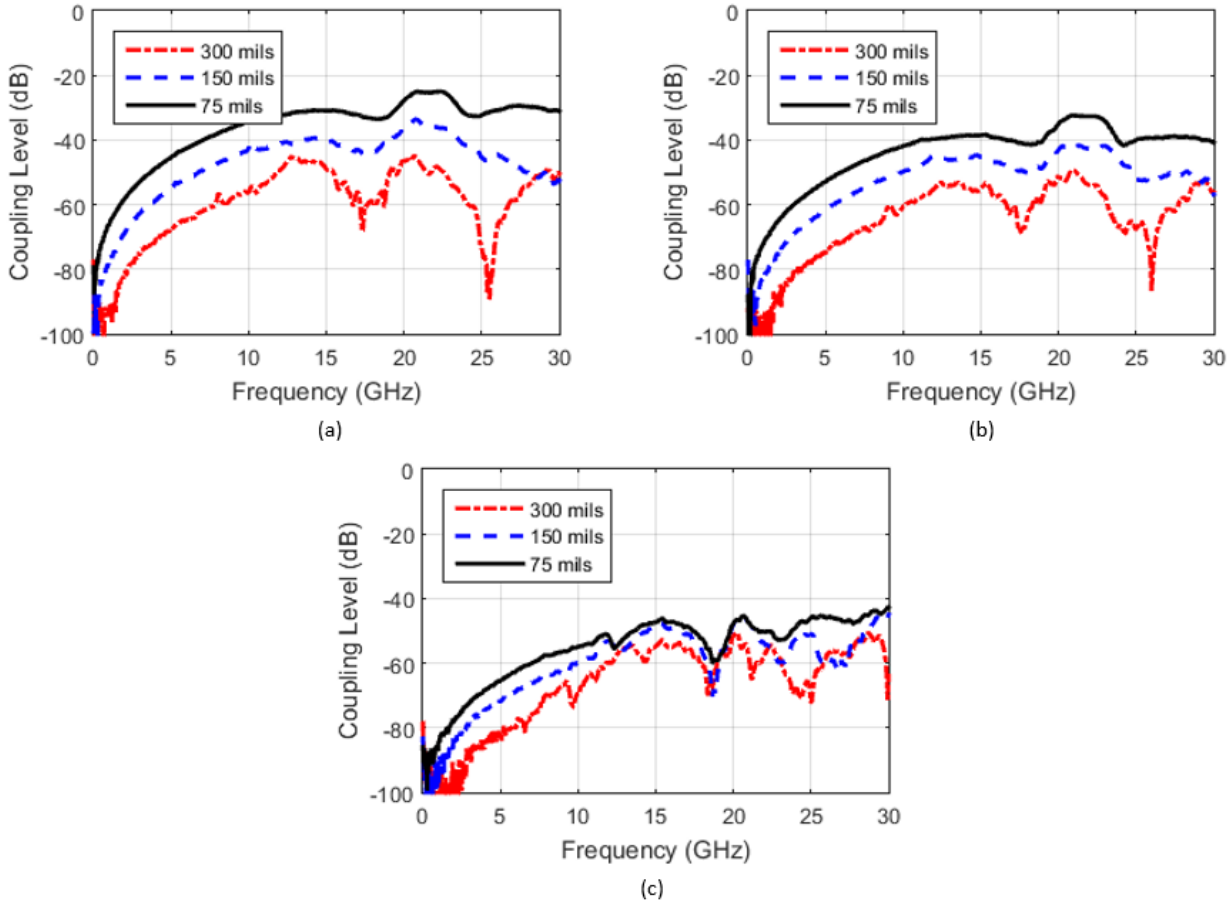

Figure 3.9 Measured Microstrip Filter to Line Crosstalk vs. Distance.
a) Microstrip Line. b) GBCPW Line. c) Stripline Line.

An important note should be made about the filters. When outside the passband of the filter, the part of the filter that contributes the most to coupling is the microstrip lead-in, which is roughly 250 mils long. When inside the passband of the filter, the resonant structures are the primary contributor to the coupling. As an example, at 10 GHz (outside of the filter passband) Figure 3.8.a shows roughly 38dB of isolation. The microstrip filter lead-in is about 250 mils, roughly ¾ of the 325 used in Figure 3.8.a. The filter and line are separated by 150 mils. From the transmission line isolation results, roughly -41dB of coupling is expected. Figure 3.9.a shows about -42dB of coupling at 10 GHz for 150 mils. As you approach the passband of the filter, the coupling caused by the resonant structures begins to dominate, increasing coupling by about 10dB for this filter which has a selectivity Q of about 10 (2 GHz bandwidth at 20 GHz center).

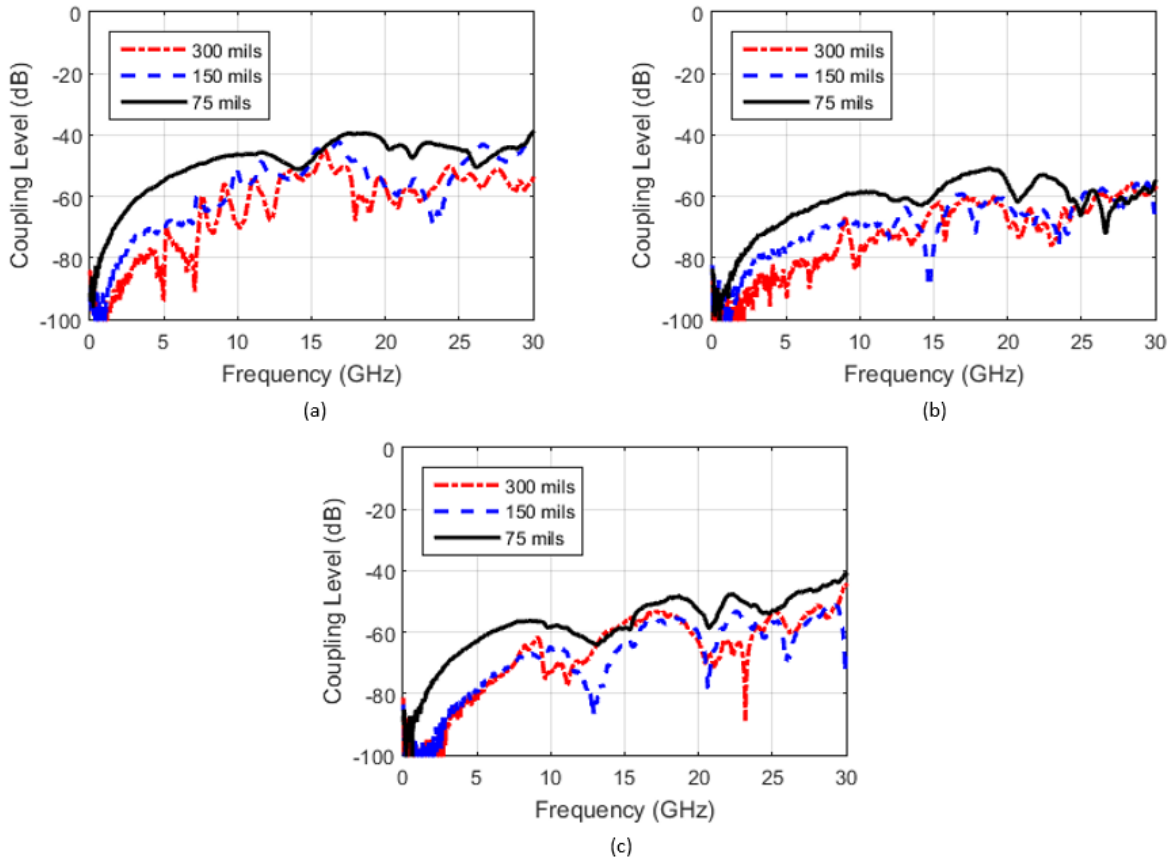

Figure 3.10 Measured Stripline Filter to Line Coupling vs. Distance.
a) Microstrip Line. b) GBCPW Line. c) Stripline Line.

Figure 3.10 shows the coupling from various transmission lines to a filter implemented in enclosed stripline. Of the three transmission lines used, stripline shows the best isolation levels with 90-100 dB of isolation through L-band and approximately 60dB of isolation within the filter passband. However, the GBCPW case appears to exhibit the best isolation across all frequencies. This is likely due to reflections and possible radiation at higher frequencies caused by the transition via, which can degrade the isolation. If the transition via used in the stripline structures is perfected, the stripline filter to stripline transmission line could be expected to exhibit the best isolation.

3.2.4 - Filter to Filter Crosstalk

Figure 3.11 shows filter to filter crosstalk for both microstrip and stripline filters. Figure 3.11.a shows a clear peak in coupling in the passband of the filters, which is caused by the resonant nature of the filter structures. The worst case isolation seen is -20dB for a separation of 75 mils. While filters would typically not be placed in proximity in an actual design, the results show that filters can significantly degrade signal isolation even for a relatively large distance of 300 mils. The isolation improves by about 10dB with each doubling of separation, which is consistent with previous findings. The coupling outside of the passband is being limited by the microstrip filter lead-ins.

In the case of the stripline filter coupling, no clear peak is seen in the passband. This is because the resonant structures are enclosed within separate stripline chambers, mitigating the crosstalk of the resonant structures. The isolation of the stripline filters is being limited by the GBCPW lead-ins. To improve isolation further, a technique to eliminate the lead-ins on layer 1 and launch a signal directly onto the stripline must be developed.

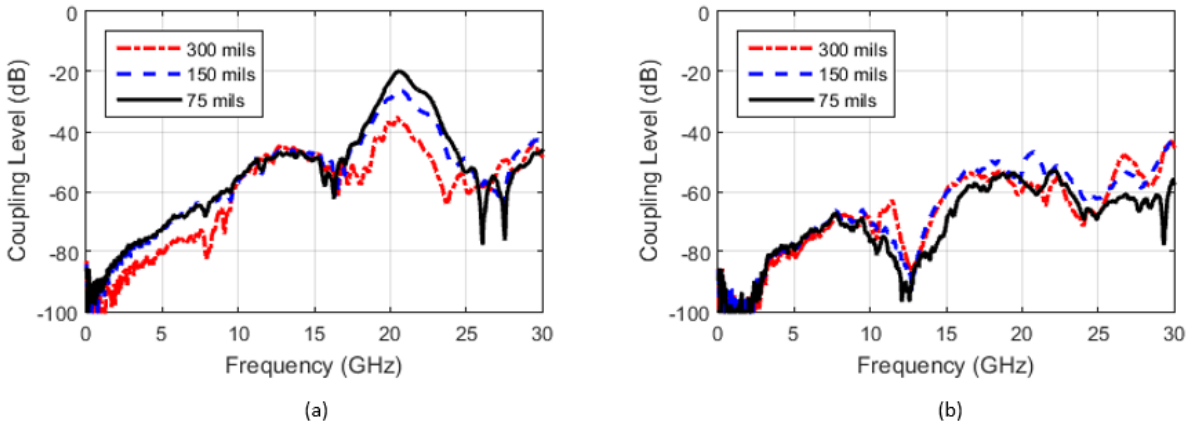

Figure 3.11 Measured Filter to Filter Coupling.

a) Microstrip Filters. b) Stripline Filters.

Chapter 4 - Electromagnetic Interference

When beginning the design of the GBCPW and stripline structures, appropriate ground via spacing was a design variable that needed to be considered. After making GBCPW structures with large via spacing, it was seen that some of the signal power was being lost at particular frequencies. That is, the power received in port 2, the power lost in the transmission line, and the power reflected back to port 1 did not equal the amount of power launched from port 1. This led us to consider that some of the signal was being radiated from the GBCPW lines. This finding is what led to this EMI study, which is still incomplete and could be the topic of future research.

4.1 - Experimental Setup

This section describes the experimental setup used to study radiation from various microwave structures. Measurements were made using a Keysight N5245A 4-port network analyzer. The test structures were connected between ports 1 and 2 of the network analyzer while a log-periodic antenna was connected to port 3. Figure 4.1 shows the radiation measurement setup using an 8-22 GHz log-periodic antenna being held approximately 1/4 inch above the test structure.

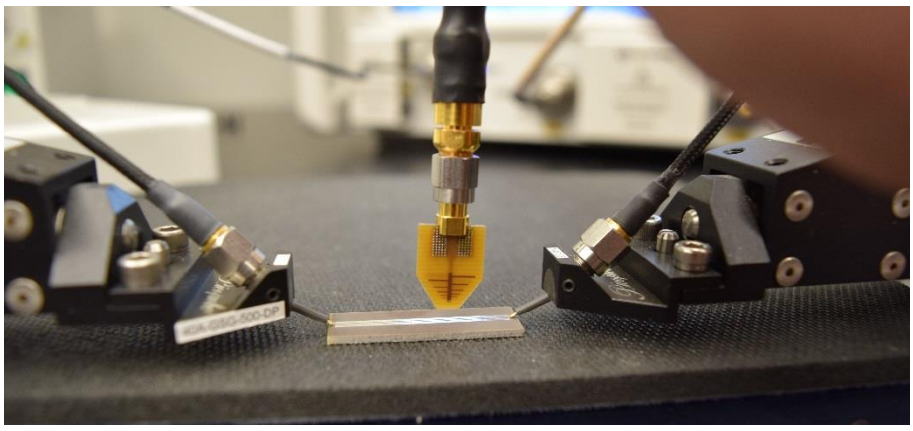

Figure 4.1 Radiation Measurement Setup.

4.2 - GBCPW Frequency Responses

The GBCPW structures used for radiation measurements were originally designed with large V_P and V_S dimensions, which are defined in Figure 2.2.b. These large dimensions created impedance discontinuities along the GBCPW lines which induce dropouts in the frequency responses. The frequencies at which the dropouts occur correspond to when V_P is equal to $\lambda/2$ and when V_S is equal to $\lambda/4$.

Figure 4.2 shows the dropouts induced by via spacing. Figure 4.2.a shows the lower frequency dropouts, which are caused by the lead-in length V_S. Figure 4.2.b shows the higher frequency dropouts, which are caused by V_P, the pitch between the vias. While not shown here, the return loss seen at the dropout frequencies is approximately 8-10 dB. This return loss did not account for the amount of power being lost in the S_{21} responses, so the antenna was employed on port 3 of the analyzer to look for possible associated radiation losses.

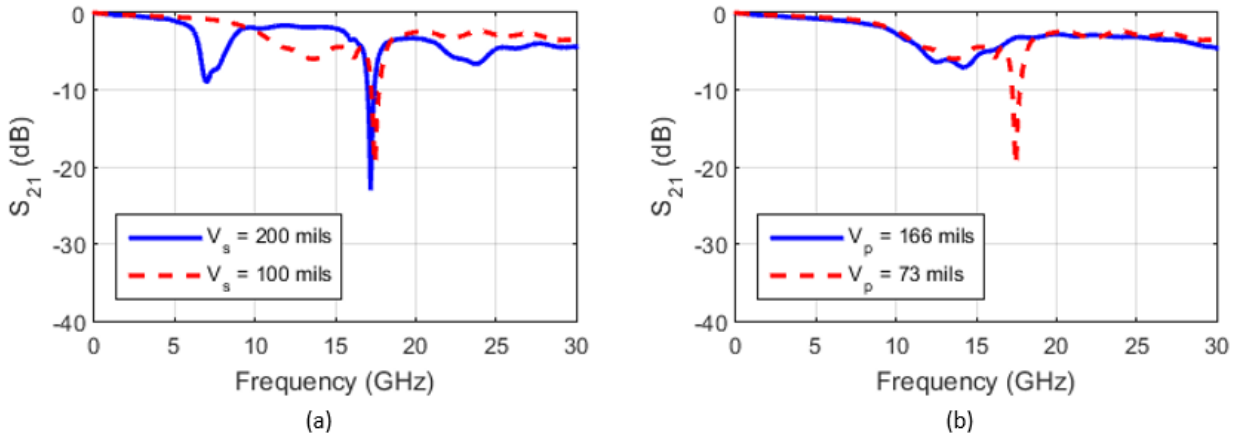

Figure 4.2 Measured GBCPW Dropouts vs. Via Spacing.
a) V_P = 166 mils. b) V_S = 100 mils.

4.3 - GBCPW Transmission Line Radiation

Where the frequency responses dip in Figure 4.2, excess radiation from the GBCPW was found to occur. Figure 4.3 shows a plot of the measured radiation from a GBCPW trace. The dashed red trace shows received radiation with a peak at the S_{21} dip corresponding to the lead-in length, V_S. The S_{31} radiation path response is close to -20dB. The dash-dotted black trace shows received radiation with a peak at the S_{21} dip corresponding to the via pitch, V_P. The S_{31} radiation path response here is approximately -30dB. These radiation mechanisms can lead to excess crosstalk in circuit boards as well as harmful interference to other electronics. With sufficient voltage on the GBCPW traces, FCC violations could also occur. The S_{21} dropouts and line radiation can be reduced by ensuring that the via spacing is sufficiently small.

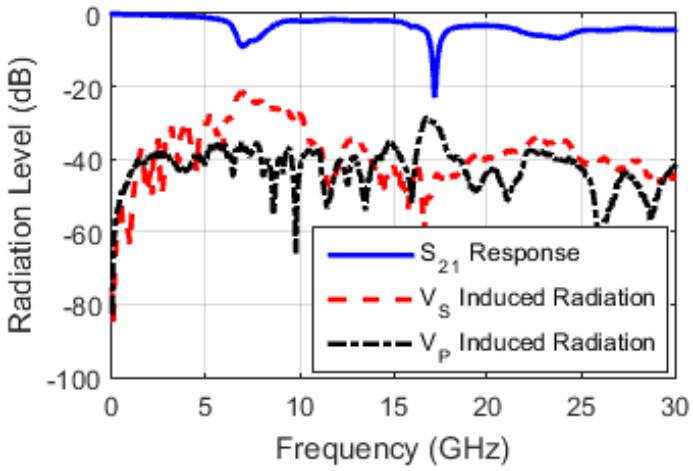

Figure 4.3 Measured Radiation from a GBCPW Trace with V_P = 186mils and V_S = 200mils.

4.4 - Filter Radiation

With resonant structures, the coupling and radiation levels are expected to increase. Figure 4.4 shows the radiation measured from the two types of filters. The microstrip filter exhibits the most radiation between roughly 8-20 GHz, while the pass band shows a slight drop in radiation.

Outside of the passband, reflections from the input of the filter are believed to be the cause of increased radiation. Inside of the passband, power passes from port 1 to port 2, which reduces reflections and hence radiation. For the stripline filter, the radiation is close to the radiation measurement floor created by the signal launch probes, so no data can be reliably extracted. This measurement floor is discussed in the next section.

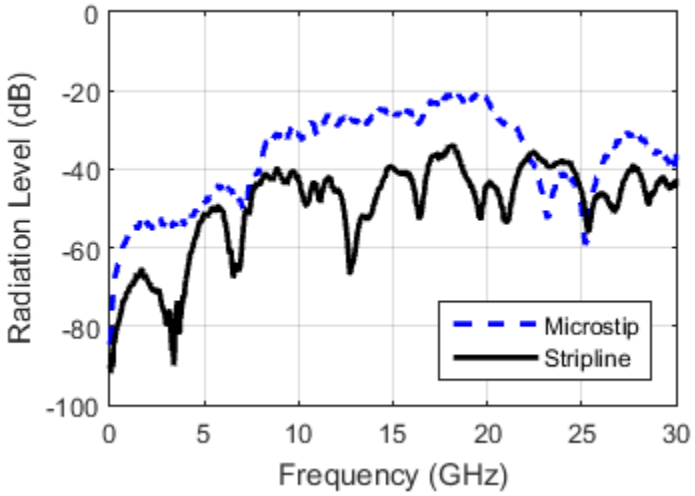

Figure 4.4 Measured Filter Radiation.

4.5 - Probe Radiation Limit

The probes used to launch the signal onto the microwave structures also emits a signal that must be accounted for in the EMI measurements. The probes are fed using a rigid coax cable. If any signal couples onto the outer shield of the coax, the internal conductor is allowed to radiate. The amount of radiation depends on how much signal couples onto the outer shield. At the tip of the probes, a transition from coax to CPW is made. This CPW also radiates a small amount. Because of these radiation mechanisms, the probes themselves create an EMI measurements floor.

To obtain the radiation floor, the probes were terminated directly into 50Ω loads and the radiation was measured using an 8-22 GHz log-periodic antenna. Figure 4.5 shows the measured

S_{31} radiation path response from the probes, indicating the measurement floor from 8-22 GHz is about -40dB at 10 GHz and above.

All of the radiation measurements taken in this chapter, except for the stripline filter radiation, are above this floor. This provides support that the radiation measurements are accurate and real. To obtain more sensitive radiation measurements, the issue of probe radiation must first be addressed. This is recommended as an avenue for future research.

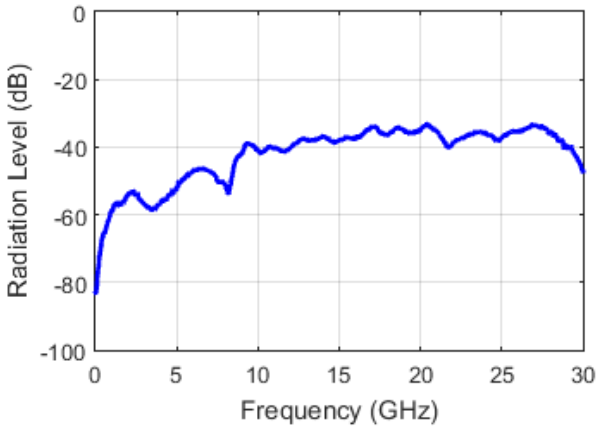

Figure 4.5 Probe Induced Measurement Floor.

Chapter 5 - Conclusions

During this research, isolation levels were studied for layout topologies comparable to what would be seen on a typical RF circuit board. The primary goal was to assess if typical RF circuit isolation goals were achievable without the use of added shielding. To achieve this goal, the isolation between several RF structures was studied based on multiple variables, such as separation distance and structure length. It was found that crosstalk on PC boards varies widely but predictably based on these variables.

The highest isolation seen in this study was achieved with stripline structures. The isolation was on the order of 100dB in the L-band, which exceeds the requirements of many RF designs. At higher frequencies, the isolation was degraded to around 60dB due to lead-in traces on the outer layers of the board. If signals can be launched directly onto stripline traces so that the outer layer lead-ins can be eliminated, the isolation could be increased at higher frequencies.

During our study, we also saw trends in isolation for the different layout variables. These trends can be used as simple guidelines to quickly assess if desired isolation is possible with given layout constraints. These trends are summarized as follows:

1) Isolation typically increases by 10-12 dB by doubling the separation between RF structures.
2) Coupling increases by 6dB for each doubling of line length.
3) GBCPW provides approximately 10dB better isolation over microstrip lines under the same layout conditions.
4) Stripline provides approximately 20dB better isolation over GBCPW under the same layout conditions.

Finally, we took a brief look at radiation from the measured structures and illustrated how issues such as via pitch in GBCPW should be carefully considered, especially at higher frequencies. Radiation from signal launches and terminations is also an important issue and can limit achievable isolation.

5.1 - Future Directions

Very good isolation through L-band using stripline structures is already possible. Future work to eliminate the lead-ins could be an area of interest, possibly providing 100dB of isolation or more at frequencies well above L-band. The primary challenge to this goal is that chips sit on the outer layers of a circuit board, requiring a transition between layers if stripline is employed. One possible solution is to embed chips so that they sit on an inner layer. This would allow the signal to launch directly onto a stripline transmission line. This would also eliminate the impedance mismatch caused by the transition via, improving performance.

Further study towards understanding EMI in microwave circuits is, therefore, a possible area of interest. To eliminate the use of added shields on circuit boards, EMI must also be reduced. Determining the primary cause of radiation on circuit boards could lead towards solutions for both higher isolation and improved EMI using only multilayer circuit board technology rather than added shielding. Hence, it is recommended that future work concentrates on studying radiation mechanisms and structures that minimize these problems.

References

[1] Bogatin, Eric. “Signal and Power Integrity – Simplified.” 2nd ed., Pearson, 2010.

[2] R. Enriquez *et al*., "Additional coupling for far end crosstalk cancellation in high speed interconnects," 2014 IEEE International Symposium on Electromagnetic Compatibility (EMC), Raleigh, NC, 2014, pp. 615-618.

[3] Johnson, Howard, and Martin Graham. “High-Speed Signal Propagation: Advanced Black Magic.” Pearson, 2003.

[4] M. M. Rana, M. R. Islam, M. K. Hosain, and A. Z. Kouzani, "Parametric investigation and measurement of near end and far end crosstalk in multiconductor microstrip transmission lines," 2011 International Conference on Applied Superconductivity and Electromagnetic Devices, Sydney, NSW, 2011, pp. 220-223.

[5] O. Ogundapo, A. Duffy, and C. Nche, "Parameter for near end crosstalk prediction in twisted pair cables," 2016 IEEE International Symposium on Electromagnetic Compatibility (EMC), Ottawa, ON, 2016, pp. 485-490.

[6] M. Kirschning and R. H. Jansen, "Accurate Wide-Range Design Equations for the Frequency-Dependent Characteristic of Parallel Coupled Microstrip Lines," in IEEE Transactions on Microwave Theory and Techniques, vol. 32, no. 1, pp. 83-90, Jan 1984.

[7] T. Zeeff, C. E. Olsen, T. H. Hubing, J. Drewniak, and D. DuBroff, "Microstrip coupling algorithm validation and modification based on measurements and numerical modeling," 1999 IEEE International Symposium on Electromagnetic Compatibility. Symposium Record, Seattle, WA, 1999, pp. 323-327 vol.1.

[8] S. Akhtarzad, T. R. Rowbotham, and P. B. Johns, "The Design of Coupled Microstrip Lines," in IEEE Transactions on Microwave Theory and Techniques, vol. 23, no. 6, pp. 486-492, Jun 1975.

[9] R. M. Osmani, "Correction to "The Design of Coupled Microstrip Lines" (Letters)," in IEEE Transactions on Microwave Theory and Techniques, vol. 28, no. 6, pp. 672-673, Jun. 1980.

[10] D. E. Bockelman and W. R. Eisenstadt, "Direct measurement of crosstalk between integrated differential circuits," in IEEE Transactions on Microwave Theory and Techniques, vol. 48, no. 8, pp. 1410-1413, Aug 2000.

[11] A. Suntives, A. Khajooeizadeh, and R. Abhari, "Using via fences for crosstalk reduction in PCB circuits," 2006 IEEE International Symposium on Electromagnetic Compatibility, 2006. EMC 2006, Portland, OR, USA, 2006, pp. 34-37.

[12] J. R. Reid, E. D. Marsh, and R. T. Webster, “Micromachined Rectangular-Coaxial Transmission Lines,” IEEE Transactions on MTT, vol. 54, no. 8, pp. 3433-3442, August 2006.

[13] W. Cui *et al*., "Lumped-element sections for modeling coupling between high-speed digital and I/O lines," IEEE 1997, EMC, Austin Style. IEEE 1997

International Symposium on Electromagnetic Compatibility. Symposium Record (Cat. No.97CH36113), Austin, TX, 1997, pp. 260-265.

[14] Lee, Thomas. “Planar Microwave Engineering: A Practical Guide to Theory, Measurements, and Circuits.” Cambridge University Press, 2004.

[15] E. Hammerstad and O. Jensen, "Accurate Models for Microstrip Computer-Aided Design," 1980 IEEE MTT-S International Microwave symposium Digest, Washington, DC, USA, 1980, pp. 407-409.

[16] Gupta, K.C., Ramesh Garg, Inder Bahl, and Prakash Bhartia. “Microstrip Lines and Slotlines.” 2nd ed., Artech House, Inc., 1996.

[17] A. Sain, K. Melde, “Impact of Ground Via Placement in Grounded Coplanar Waveguide Interconnect,” IEEE Trans Comp Pack Manu Tech, pp. 136 – 144, vol. 6, no. 1, Jan 2006.

[18] D. M. Pozar, “Microwave Engineering.” 4th ed., Wiley, 2012.

[19] W. Liu, Z. Zhang, Z. Feng and M. F. Iskander, "A Compact Wideband Microstrip Crossover," in IEEE Microwave and Wireless Components Letters, vol. 22, no. 5, pp. 254-256, May 2012.

Appendix A - Supplemental Information

The information in this appendix is provided in order to increase the understanding of the techniques used to arrive at the coupling results discussed in this thesis.

A.1 - Scattering Parameter Background

One classical approach to characterizing electrical systems is with the use of H-parameters. H-parameters describe an electrical system in terms of its input and output voltages and currents. This generates the input and output impedances as well as the forward and reverse gains of the system being characterized. To determine the H-parameters, the input and output of the system are required to be open or short circuited. The creation of an accurate open or short circuit at high frequencies is extremely difficult due to parasitic capacitance and inductance. Also, some systems can become unstable under open or shorted conditions. Various other characterization parameters have been developed, such as Z-parameters or Y-parameters, which use similar measurement techniques.

Enter Scattering parameters, or simply S-parameters. Unlike the other characterization techniques mentioned, which directly measure voltage and current, S-parameters measure the incident and reflected waves at the input and output ports of the systems. For these measurements, S-parameters do not require the input and output of the system to be shorted or open. Rather, the ports are terminated with the systems characteristic impedance, Z_o, which is typically 50Ω in RF systems. Because the characteristic impedance is purely resistive, it does not change with frequency, and the parasitic inductances and capacitances have a much less significant impact. For instance, when terminating the output with an open load, if the impedance of the parasitic capacitance changes from 10MΩ to 10kΩ the system characterization using H-parameters would

be inaccurate. However, when terminating the output with 50Ω, the parasitic capacitance is in parallel with the 50Ω and the termination impedance would be left relatively unchanged.

Before defining what S-parameters are and how they are used, a bit of transmission line theory is in order. Using [18] as a reference, Figure A.1 shows a model for an arbitrary lossless transmission line with a characteristic impedance, Z_0, and signal phase shift constant, β. The line is terminated with a load impedance Z_L. As a signal, $V(x), I(x)$ is initially launched onto and propagates down the line, $V(x) = I(x)Z_0$. Then, when the signal reaches the load, $V(x) = I(x)Z_L$ must also hold true. If $Z_0 \neq Z_L$, how can these equations be equal? The answer is that some of the signal is reflected back down the transmission line towards the source in the –x direction.

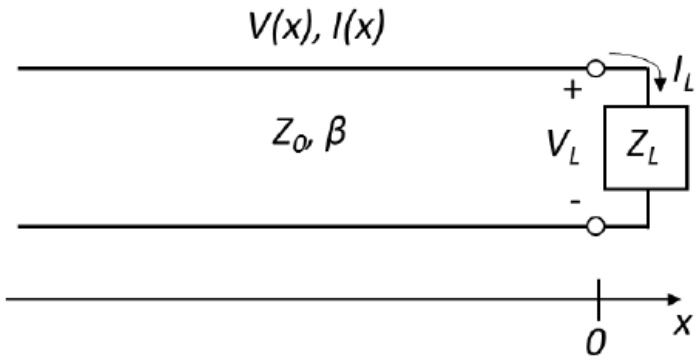

Figure A.1 Lossless Transmission Line Terminated in a Load Impedance.

Let us call the forward traveling wave V^+ and the reverse traveling wave V^-, then the voltage at any point on the line is given with (A.38). Similarly, the current at any point is given by (A.39). Then, using Ohm's law, (A.40) provides impedance of the transmission line.

$$V(x) = V^+ e^{-j\beta x} + V^- e^{-j\beta x} \tag{A.38}$$

$$I(x) = \frac{V^+}{Z_0} e^{-j\beta x} - \frac{V^-}{Z_o} e^{-j\beta x} \tag{A.39}$$

$$Z_L = \frac{V(0)}{I(0)} = \frac{V^+ + V^-}{V^+ - V^-} Z_o \tag{A.40}$$

Finally, by rearranging (A.40) and solving for V^-/V^+, (A.41) can be used to determine the ratio of reflected and forward voltages. This parameter, Γ, is known as the reflection coefficient and is at the heart of S-parameters.

$$\Gamma = \frac{V^-}{V^+} = \frac{Z_L - Z_o}{Z_L + Z_o} \tag{A.41}$$

Now, to define the S-parameters of a 2-port system, the setup in Figure A.2 is typically used. In the model, a_1 and a_2 represent incident waves heading towards the system while b_1 and b_2 represent waves moving away from the system.

Figure A.2 2-Port Network Model.

(A.42) and (A.43) provide the relationships between the traveling waves and the S-parameters. It is easy to see that by setting either a_1 or a_2 equal to zero each S-parameter can be found.

$$b_1 = S_{11}a_1 + S_{12}a_2 \tag{A.42}$$

$$b_2 = S_{21}a_1 + S_{22}a_2 \tag{A.43}$$

To set a_1 or a_2 to zero, any reflections caused by the source and load must be eliminated. From (A.41), $\Gamma = 0$ when $Z_L = Z_o$. In this 2-port system, by setting Z_S and Z_L equal to the ideal characteristic impedance of the system there will be no reflections caused by the source or load. If the source and load impedances are properly matched, then S_{11} gives the input reflection coefficient, S_{22} gives the output reflection coefficient, S_{21} gives the forward gain, and S_{12} gives the reverse gain of the system.

$$S_{11} = \left.\frac{b_1}{a_1}\right|_{a_2=0} \tag{A.44}$$

$$S_{22} = \left.\frac{b_2}{a_2}\right|_{a_1=0} \tag{A.45}$$

$$S_{21} = \left.\frac{b_2}{a_1}\right|_{a_2=0} \tag{A.46}$$

$$S_{12} = \left.\frac{b_1}{a_2}\right|_{a_1=0} \tag{A.47}$$

A.2 - What's a little stub got to do with it?

RF circuit board design is filled with "gotchas" that can be painfully discovered by the inexperienced. Transitioning a signal between layers of PC boards appears trivial, and can be at low frequencies. At higher frequencies, though, many considerations must be made. Layer transitions on PC boards have been the topic of several studies, such as [19]. Close study and accurate design of via transitions are important since, from the previous section, changes in impedance can cause signal reflections and seriously degrade performance. Many studies involve

analyzing how a via changes the characteristic impedance of the line and how to best design the via to avoid this. Another important consideration is the via stub.

Figure A.3.a shows one possible layout of a stripline transmission line, similar to the one seen in Figure 2.2.c. The important difference being that the internal trace is now on layer 2 rather than layer 3, leaving a 52 mil stub. Figure A.3.b shows the frequency response of this stripline with a large dropout in S_{21}. Signal reflections caused by the via stub become significant at approximately 5 GHz, and creates a large dropout at 21 GHz. At 5 GHz, the via stub is only $\lambda/20$ in length. This means that when a transition is made to or from an internal layer, the via stub should be kept shorter than $\lambda/20$ to avoid strong reflections, and under $\lambda/4$ to avoid total dropouts.

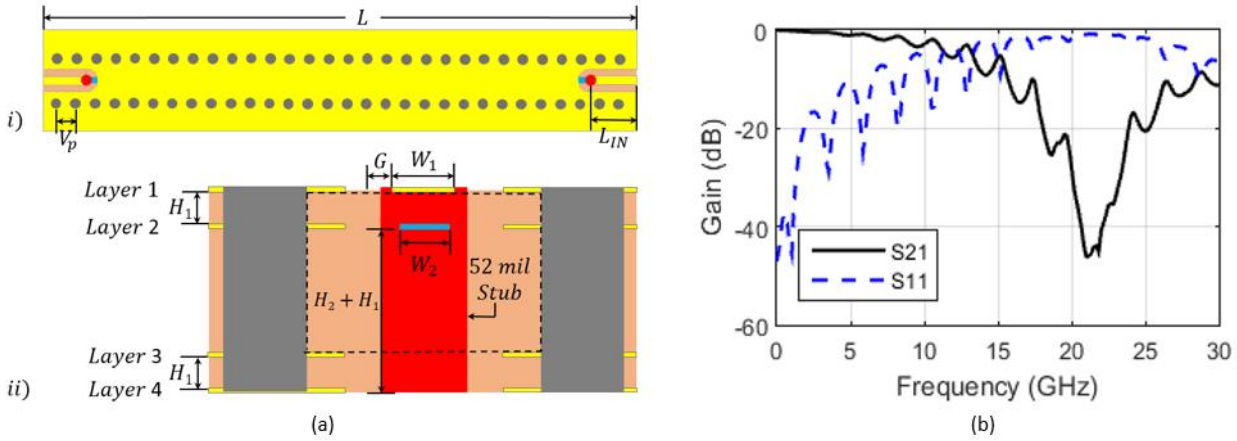

Figure A.3 Via Induced Dropout in S_{21}.

a) Stripline Dimensions. b) Stripline Frequency Response.

i) Top View. ii) Cross Section.

If, however, the internal trace is on layer 3, the stub is only 10 mils in length moving the dropout above 25 GHz. This is the reason dropouts were not seen previously in Figure 3.3.b. Of course, the stub can be avoided all together if blind or buried vias are employed. This option typically involves a hefty surcharge by manufacturers. Another, cheaper alternative is back-

drilling. This process simply involves drilling out the unused portion of the via, which removes the stub.